Role of Dissolved Gas in Optical Breakdown of Water: Differences between Effects Due to Helium and Other Gases

N. F. Bunkin,*,† B. W. Ninham,§ V. A. Babenko,‡ N. V. Suyazov,† and A. A. Sychev‡

A.M. Prokhorov General Physics Institute, Russian Academy of Sciences, ul. Vavilova, 38, 119991, Moscow, Russia, Lebedev Physical Institute, Russian Academy of Sciences, Leninskii pr. 53, 119991, Moscow, Russia, and Department of Applied Mathematics, Research School of Physical Sciences and Engineering, The Australian National University, Canberra, ACT 0200

Received: February 24, 2010; Revised Manuscript Received: May 11, 2010

It is shown that water contains defects in the form of heterogeneous optical breakdown centers. Long-living complexes composed of gas and liquid molecules may serve as nuclei for such centers. A new technique for removing dissolved gas from water is developed. It is based on a "helium washing" routine. The structure of helium-washed water is very different from that of water containing dissolved atmospheric gas. It is able to withstand higher optical intensities and temperatures of superheating compared with the nonprocessed ones. The characteristics of plasma spark and values of the breakdown thresholds for processed and nonprocessed samples are given.

1. Background

The nature of defects in water structure induced by dissolved atmospheric gas is a matter that remains open. The effects of such defects and their interplay with specific ion effects on colloidal particle interactions, interfacial tensions, and bulk solutions of electrolytes has hardly been considered by theorists. A large literature exists on hydrophobic and Hofmeister effects,[1–7] on surface phenomena,[8–12] and on simulation of the properties of water and electrolytes.[13–18] The simulations ignore dissolved gas, yet the experiments with which simulations are compared involve water and solutions that contain dissolved gas.

The same is true for complementary approaches. New theoretical developments recognize that classical theories of intermolecular forces based on electrostatic interactions alone are flawed because of omission of quantum mechanical dispersion forces (see, e.g., refs 19 and 20). Yet again, the theories ignore gas effects. The problem is ubiquitous in physical chemistry.

The fact that dissolved gas can have a large yet unknown role to play can be inferred from a number of direct and indirect observations: At the air−water interface, atmospheric gas density changes from that at 1 atm (1 molar concentration) to $\sim 5 \times 10^{-3}$ molar in the bulk, a transition that occurs over a few molecular layers. This must have some effect in understanding tensions and changes due to dissolved salts.[21–27] Rates of flocculation of hydrophobic colloids change by orders of magnitude when atmospheric gas is removed. Emulsions from which dissolved gas is removed become stable or at least much less unstable.[28–36] The list can be expanded.

Such phenomena implicate defects in water because of sparingly soluble impurities in the hydrophobic effects. The defects change the nature of water qualitatively. Perhaps the most remarkable unexplained phenomena are experiments on bubble−bubble interactions and their specific ion and concentration dependence. There is an interplay between gas and electrolyte ions in mediating long-range interactions and bubble fusion.[37] Most phenomena on which attention is focused in colloid science and biology involve electrolytes at concentrations that range typically from 10^{-3} to 0.1 M. Dissolved atmospheric (hydrophobic) gas molecules under normal conditions are at concentrations around 5×10^{-3} M (see, e.g., refs 38–40). The fact that there is an interplay between dissolved gas and electrolytes is clear from measurements of gas solubility, which is ion specific and varies in a wide range of the content of salt.[41–45]

It has been known for over a century that the tensile, (rupture) strength of water containing dissolved atmospheric gas is orders of magnitude less than that which is predicted theoretically (see, e.g., ref 46). That is consistent with solid-state physics where the strength of materials is determined primarily by defects in the lattice.[47] In the solid-state atomic or isotopic impurities associate to form larger multimolecular aggregates. It is not stretching matters too far to imagine that such aggregates will also form in the disordered dynamic lattice that is water. The presence of microscopic gas cavities in a liquid under normal conditions arises, for instance, at explaining the experimental results on acoustic cavitation in liquids and sonar chemistry generally. Indeed, experimentally observable cavitation thresholds (values of negative pressure resulting in the cavitation bubble appearance in liquid media) occur in the range of 1−10 atm, whereas the rupture strength of a liquid is estimated to be $\alpha n^{1/3} \approx 10^4$ atm, where α is the surface tension factor of the liquid and n is the number of molecules of liquid per unit volume (see, e.g., ref 48). The discrepancy between the theoretical estimate and observed threshold for acoustic cavitation leads to the assumption that even in a settled and purified liquid there may exist stable micrometer-sized bubbles of the dissolved gas, which can act as cavitation centers. Such a conclusion is still open.

Nonetheless, the problem of the nature of defects due to gas molecules, whether they be dispersed as molecules, aggregates of microbubbles, or both, remains frustratingly elusive. The rehearsal above shows that the effect of such defects on the

* Corresponding author. E-mail: nbunkin@kapella.gpi.ru.
† A.M. Prokhorov General Physics Institute.
‡ Lebedev Physical Institute.
§ The Australian National University.

10.1021/jp101657f
Published on Web 05/24/2010

properties of "water" and more importantly on colloidal interactions can be qualitatively large and at variance with theories and simulations in physical chemistry. Any probe of structure that provides insight has to be useful. At a technical level, the removal of dissolved gas to give easily useable experimental "water" that provides a real model against which we test theories is cumbersome. Freeze thaw cycles, in principle, do the job but require hard work. We have developed a technique of helium washing that seems to offer some prospects.

Before describing the technique and results, we shall note that some previous works of ours involving laser probes of liquid samples were published in refs 49–52. These works were devoted to experimental verification of the so-called "bubston" concept.[53,54] Bubstons (an abbreviation of "bubbles stabilized by ions") are stable gas bubbles in a liquid with ionic conductivity and saturated with dissolved gas. By our estimations, the radius of a bubston in water is ~100 nm. It has been shown[54] that bubstons are capable of coagulating with one another to form bubston clusters; the radius of these clusters, according to our estimates, is ~500 nm. As demonstrated in our recent work,[55] it is possible to observe these clusters via angular scattering of laser radiation and the technique of modulation interference microscopy; the results of that experiment can be interpreted to be direct proof of the existence of bubstons and bubston clusters in water samples saturated with dissolved gas (e.g., atmospheric air) and containing trace amounts of ions.

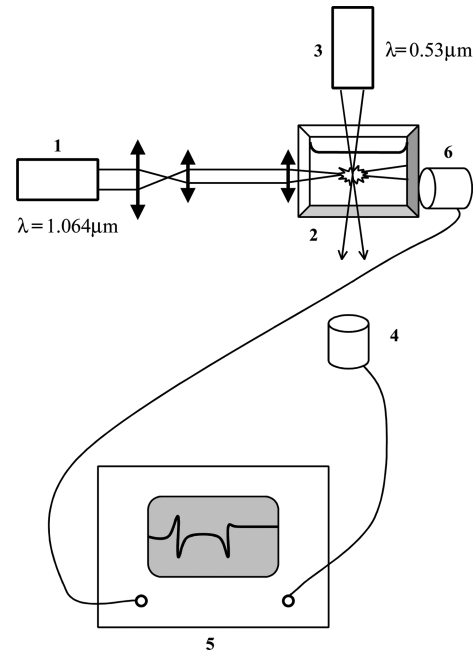

Figure 1. Schematic of the detection of scattered optical radiation and acoustic signal: (1) single-mode repetitively pulsed YAG/Nd^{3+} laser; (2) cell with liquid; (3) frequency doubled single-mode cw YAG/Nd^{3+} laser; (4) differential split photodetector; (5) digital oscilloscope; (6) piezoelectric sensor.

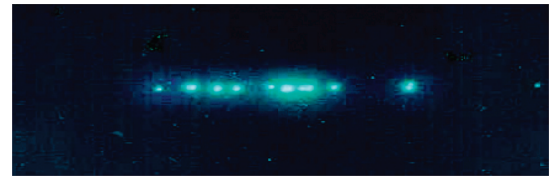

Figure 2. Photo of the breakdown flash in the sample of water.

2. Experimental Results and Discussion

In the present study, an experiment on the interaction of intense optical radiation with such (presumed) bubston clusters is described. As was shown in our theoretical study,[56] such an interaction may result in low-threshold optical breakdown of the liquid. Low-threshold laser-induced breakdown is an occurrence of a plasma spark at the focus of the laser beam. The breakdown threshold (as related to the intensity of radiation) is two to three orders less than the value corresponding to the development of multiphoton ionization in media (optical breakdown resulting from the process of multiphoton ionization can be considered as high-threshold breakdown, as described in a comprehensive report of the different models of the optical breakdown in water[57]). The characteristic feature of low-threshold breakdown is its sporadic character; that is, it arises only with certain probability, W. This unequivocally indicates that low-threshold breakdown is initiated by the breakdown centers occasionally moving inside the focal volume, V, whereas this volume is defined by the energy of the pulse and focusing conditions. Because these experiments were performed with liquids filtered through a membrane filter with an effective pore size of ~100 nm, the liquid samples were free of any colloid particles. Therefore, it is possible that these breakdown centers are bubston clusters moving as do Brownian particles. The probability of the appearance of at least one of these clusters inside the focal volume is defined by the volumetric density, n_{cl}, of the clusters. According to the Poisson distribution,[72] the theoretical value of the probability of such event is $W_{theor} = \sum_{m=1}^{\infty} \exp(-n_{cl}V)((n_{cl}V)^m)/(m!) = [1 - \exp(-n_{cl}V)]$, where $n_{cl}V$is the average number of the bubston clusters inside the volume, V. The breakdown will happen provided that the radiation intensity inside the volume, V, exceeds some threshold value, specific for the breakdown by the bubston cluster mechanism (cf. our previous theoretical study[56] for more details). The experimentally measured breakdown probability is defined by the formula $W_{exp} = N_{br}/N_p$, where N_{br} is the number of breakdown flashes and N_p is the total number of laser pulses, counted within some time of laser shooting. At $n_{cl}V \ll 1$, $W_{theor} \approx n_{cl}V \approx W_{exp} = N_{br}/N_p$. In other words, the value of W_{exp} is just proportional to the density of bubston clusters, n_{cl}. In what follows, we describe the experiments on sporadic optical breakdown.

2.1. Experimental Setup. A cell with a liquid under study was mounted on an optical bench and then was irradiated by laser pulses. The scheme of the experimental setup is shown in Figure 1. Here we used a pulse-repetition YAG/Nd^{3+} laser (1) operated in the Q-switching TEM_{00} mode; the wavelength was $\lambda = 1.064$ μm, pulsewidth τ was 11 ns, pulse repetition frequency was 2 Hz, and energy of the pulses can be varied from 10 to 15 mJ by using multicascade amplifiers. The focusing conditions and laser pulse energy were chosen in such a way that breakdown was not induced by each laser pulse; that is, the conditions for the regime of sporadic breakdown were met. The laser pulses were directed by means of a telescope and a system of lenses to cell (2) with a liquid where the optical breakdown was excited. The breakdown appeared at a depth of 5 mm from the liquid surface. Radiation was focused into a spot of diameter 0.3 mm in the neck of a caustic inside the liquid sample by a lens with a focal distance of 15 cm. Therefore, the radiation intensity was varied in the range (0.13 to 0.2) $\times$ 10^{10} W/cm^2.

The optical breakdown produced by laser pulses was accompanied by a bright flash, illustrated in Figure 2, and the appearance of a macroscopic cavitation bubble. The photo in

Figure 2 was taken with the help of a micro-objective, not shown in Figure 1. As seen in this photo, the pattern of breakdown flash consists of multiple separate sparks distributed along the caustic having a length of several millimeters. It may be assumed that each spark is related to the breakdown of a single cluster of bubstons, and all of these clusters appeared in the caustic during the laser pulse. Additionally, the plasma sparks shielded the incident laser light only slightly, and ~90% of radiation goes behind the caustic. The sound appearing during the breakdown and subsequent collapse of a cavitation bubble modulates the refractive index of water, which causes the deviation of the probe beam from its initial direction. This deviation was measured with the differential optical sensor (4) consisting of two split photodiodes and sensitive to the probe-beam deviations. The output signal of sensor (4) was fed to one of the channels of Tektronix TDS-540 digital store oscilloscope (5). An acoustic piezoelectric sensor (6) based on a textured piezoelectric film, described in ref 59, was pressed against the cell. The film thickness was 20 μm, and its resonance frequency was 22 MHz. The output signal of this sensor was fed to another channel of the oscilloscope. Therefore, we could observe for one laser pulse simultaneously both the signal of the scattered probe radiation and the acoustic signal. The oscilloscope was triggered by the pulse that opened the electro-optic gate of a pulsed laser; that is, it operated synchronously with the laser pulse. The oscilloscope was connected to a computer via a GPIB board for accumulating and digital processing of experimental data. The data array was formed by the output signals of sensors (4) and (6).

The method of detecting the breakdown is based on the study of the cavitation bubble dynamics, which is well developed (see, for example, ref 58 and references therein), and the breakdown probability can be simply determined by measuring the probability of appearance of such a bubble. This method is based on the refraction of the probe beam of a cw laser in the acoustic wave field appearing first during the optical breakdown and then during the collapse of a cavitation bubble. For this purpose, the breakdown region was irradiated by focused probe 0.53 μm, 40 mW second harmonic from a cw YAG/Nd^{3+}-laser (3) perpendicular to the first harmonic radiation beam. (See Figure 1.) The beam diameter in the focus did not exceed 50 μm. Note that the mutual location of the probe-beam waist and optical breakdown flash was not critical: the probe beam could be displaced within 5 mm above and below the flash region.

Figure 3 presents oscillograms obtained from a differential split photodiode sensor (optical detection channel (4)) and an acoustic sensor (acoustic detection channel (6)). One can see that in both cases, the signal consists of two distinct pulses. The first pulse is caused by the optical breakdown, shock-wave generation, and the appearance of a cavitation bubble. The shock-wavefront deflects the probe cw laser beam, resulting in the appearance of a signal on the differential split photodiode sensor (4); the same shock wave also excites the acoustic sensor (6). It is known[48] that a cavitation bubble formed during optical breakdown first increases, achieving the maximum size, and then collapses. During the collapse, a shock wave is generated once again, which is detected, as before, with two sensors (4) and (6). One can see that the time interval between pulses in both detection channels is the same. This confirms the validity of the method of parallel detection of the optical breakdown by the probe-beam deflection and by the acoustic pulse.

It is interesting to note that the time interval, Δt, between the first and the second pulses in the optical and acoustical channels of measurements (Figure 3) depends on the magnitude

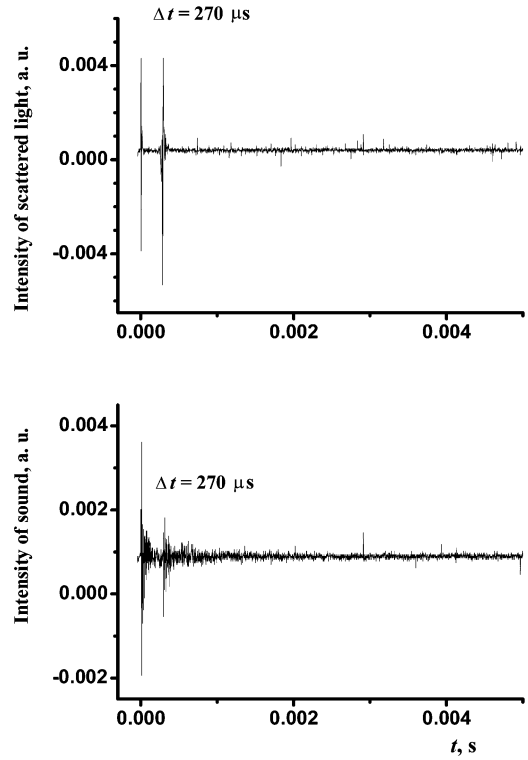

Figure 3. Oscillograms of the optical (a) and acoustic (b) signals.

of the pressure inside the cell. For instance, we have $\Delta t = 270$ μs in the case when $p = 1$ atm, whereas at decreasing the value of $p - p_{sat}$, the time interval Δt grows. (See Figure 4a,b). As is known,[60] the time of collapse of the Rayleigh cavity is connected to energy of the cavitation bubble, E_b, by the relation

$$\Delta t = 1.14\rho^{1/2}E_b^{1/3}(p - p_{sat})^{\alpha}$$

where the exponent $\alpha = -5/6$ and ρ is the density of water. As is seen from Figure 4 for both the optical and acoustic sensors (4) and (6), the experimental points belong to the same straight line, having a tangent of slope equal to $-0.84 \approx -5/6$. Therefore, by measuring the time intervals, Δt, we can develop a technique for a noncontact measurement of the liquid pressure inside hermetic vessels, transparent for laser radiation and containing liquid samples. This, however, is outside the scope of the given study.

The data array was processed as follows. The necessary condition was the appearance of two rather intense pulses in both detection channels ((4) and (6)), which should be separated by the same time interval. The method allows reliable detection of the breakdown. The breakdown probability was determined from these data in a series of 10 successive measurements; each measurement involved 5 min of laser shooting. In fact, a computer directly counted the number, N_{br}, of breakdown flashes during each series of measurements; the value of $W_{exp} = N_{br}/N_p$ was calculated as the average of each series.

2.2. Preparation of Samples. Water was carefully purified in an ion-exchange resin rectification column; the specific resistance was 5 MΩ·cm, which was measured just before each series of laser shooting. Additionally, we tested the magnitude of pH, which was equal to 6.7 to 6.8, that is, water samples possessed by slightly acidic properties. The aqueous samples were prefiltered as well; we used porous membrane filter with the size of a pore of ~100 nm. The samples of water were stored

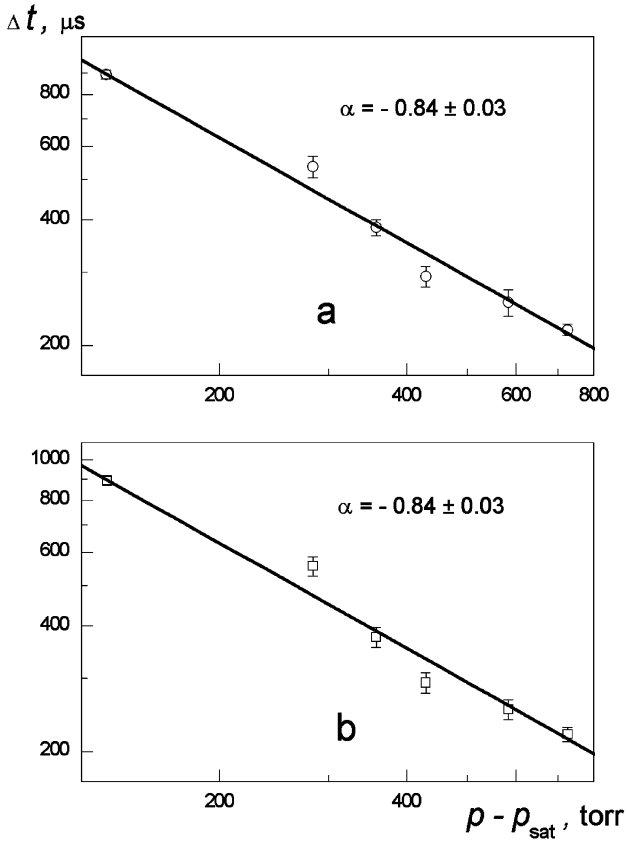

Figure 4. Dependence of the delay time, Δt, for the second pulse relative to the first one on the pressure difference $p - p_{sat}$ for the (a) optical and (b) acoustic sensors (statistical weight for the value of Δt is inversely proportional to the error).

in nontransparent blackened (to avoid the influence of daylight) flasks made of fused silica or Teflon and supplied with press caps to keep the sample away from penetration of carbon dioxide and dust particles; note that the magnitudes of specific resistance and pH were not changed during storage in the flasks. Then, the sample was poured in a hermetic transparent cylindrical cell made of fused silica with a volume of 150 mL and diameter of 40 mm; the hermeticity was provided by vacuum valve. In fact, during the measurements, we could not control for the daylight factor. The cell was manufactured paying special attention to the elimination of possible contamination sources. For this purpose, the windows of the cell, through which radiation was input and output, were welded (i.e., we did not use a glue to fix the windows), and the vacuum-valve rod was made of Teflon. The cell design allowed the measurements of the resistance and temperature of water with the help of black platinum electrodes located in a Teflon plug and a thermal resistor in a quartz capillary; in fact, this thermal resistor was not in contact with the water sample (just to avoid possible contamination of a liquid sample) but measured the temperature of the cell face. At the same time, the cell was not supplied with an ion-selective electrode for measuring the pH value, as the liquid sample should be exerted to very high pressure (see below), and such an electrode could be damaged. The cell was half filled. Experiments were performed with aqueous samples kept in atmospheres of N_2, O_2, Ar, He, NO, Ne, H_2, and C_2H_6; see below. All gases were of analytical grade. In what follows, we describe the degassing procedure for the water samples and then present the results of experiments.

2.3. Degassing. Degassing was performed in several stages; each stage had the corresponding number $N = 1, 2$, and so on. In the first stage, the cell with a free volume filled with atmospheric air at the pressure $p = 1$ atm was connected to a backing pump for 10 s (this time was sufficient for a complete evacuation of the free volume of the cell), and a pressure of 10^{-3} Torr was produced in the free volume. During this process, special attention was paid to avoid contaminating the sample. In fact, we did not connect the cell directly to the backing pump but instead to the bypass chamber of a large volume, which was evacuated beforehand. Therefore, the possibility for the droplets of the backing pump oil to penetrate the sample was excluded.

Then, the vacuum valve was closed, the pump was disconnected, and the resistance and temperature were measured. The temperature measured immediately after pumping out was below the initial temperature, which is explained by the evaporation of water during pumping out; whereas the resistance values had a large scatter. This is probably explained by the fact that the electrode surface was covered with bubbles (which can be observed with a microscope). After 10−15 min, the temperature and resistance acquired the initial values. Then, the liquid was allowed to settle for a day; during this time, the free volume was filled with vapor, allowing some amount of dissolved gas to escape from the liquid. After 24 h, the settling pressure, p, and probability, W_{exp}, were measured. Measurements of these magnitudes indicated the termination of the first stage of degassing. The second and subsequent stages ($N = 2$, 3, etc.) also involved 10 s of evacuating with subsequent hermetic sealing and daily settling; upon termination of each stage, the values p and W_{exp} were also measured. The results of measurements are shown in Figure 5a,b as a function of the stage number, N. It can be observed that pressure, p, inside the free volume decreases with increasing N, reaching a stationary level at $N = 3$ to 4. This stationary level is related to the saturated vapor pressure ($p_{sat} = 17.5$ Torr) at room temperature. The fact that the stationary level of the residual pressure, p, results after 75−100 h of degassing is in agreement with the estimated diffusion time, τ_d, of the dissolved nitrogen from a volume of water with depth $h \approx 20$ mm: $\tau_d \approx h^2/D_g \approx 85$ h. ($D_g \approx 1.3 \times 10^{-5}$ cm^2/s is the diffusivity of nitrogen in water at room temperature.)

In our opinion, the establishment of p_{sat} in the free volume does not mean that water appears completely free of dissolved gas. Indeed, molecules of dissolved gas escaping the liquid should overcome the potential barrier caused by interaction with the nearest molecules of liquid, and this process occurs over a time $\tau_{overcome}$, for which the condition $\tau_{overcome} \gg \tau_d$ is met. We assume here that we are dealing with the solvates of dissolved gas (the combinations of solvent molecules with molecules of water), which have an anomalously long lifetime. This is why the saturated vapor pressure, p_{sat}, established in the free volume of the cell does not mean that all of the molecules of dissolved gas have left the liquid sample.

This assumption is confirmed by the subsequent measurements of p and W_{exp}. As shown in Figure 5b, the probability W_{exp} initially falls at increasing N, but at $N = 4$, when $p \approx p_{sat}$, W_{exp} drastically increases and remains high as N increases. Our interpretation of these results is that as the liquid begins to boil at $p = p_{sat}$ and vapor bubbles, the centers of optical breakdown, are generated on the remaining solvates of dissolved gas molecules (heterogeneous nuclei); here we should take into account the fact that the radiation at the given wavelength is slightly absorbed by water (its absorptivity is 0.16 cm^{-1}), which shifts the liquid in the local area of laser shooting to the superheated state. Therefore, the vapor bubbles are formed and

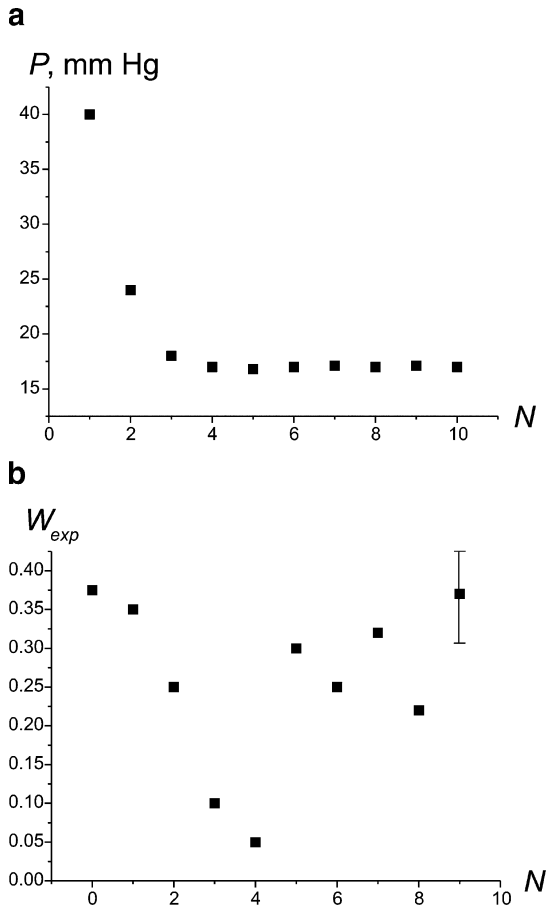

Figure 5. (a) Dependence of pressure, p, as a function of the number of degassing stage (point p (0) is excluded). (b) Dependence of probability, W_{exp}, as a function of the number of degassing stage. Value W_{exp} (0) corresponds to the probability measured under normal conditions.

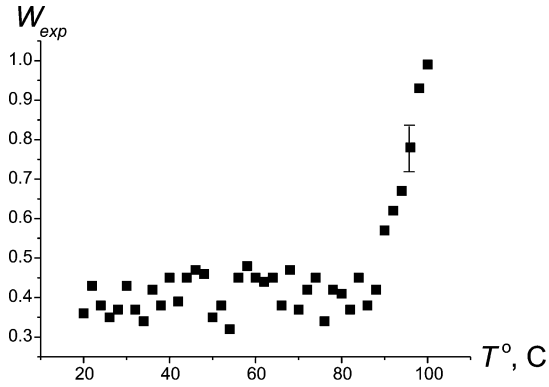

Figure 6. Dependence of probability, W_{exp}, as a function of temperature.

serve as additional centers for optical breakdown, resulting in the increase in breakdown probability. This assumption was experimentally verified by measuring the probability, W_{exp}, of optical breakdown as a function of temperature, T; the intensity of radiation and focusing conditions were the same as in the previous case. As shown in Figure 6, the breakdown probability does not depend on temperature critically within the entire range of measurements up to $T = 97$ °C, where the value of W_{exp} increases considerably. This confirms our hypothesis that far from the boiling point the gas bubbles serve as the centers for optical breakdown, whereas close to the boiling point, these centers include both gas and vapor bubbles. Therefore, to

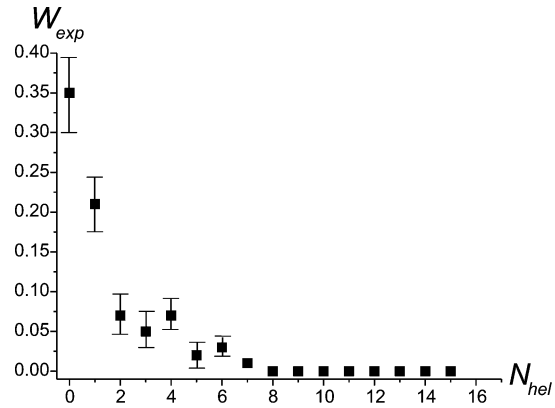

Figure 7. Dependence of probability, W_{exp}, as a function of the number of "helium washing". Value W_{exp} (0) corresponds to the probability measured in the evacuated but not helium-washed sample of water.

suppress low-threshold optical breakdown, it is necessary to completely remove the heterogeneous nuclei for gas and vapor bubbles. As previously mentioned, we assume that these nuclei are the long-living solvate molecules of the dissolved gas, which serve as local defects in the molecular arrangement of the liquid (liquid matrix).

2.4. Helium Washing. The assumption of the existence of long-lived solvates of a dissolved gas stimulated our additional experiments with the aim of finding the dependence of this hypothetical effect on the type of a gas. In the first experiment, we developed the following procedure. We pumped helium, at pressure of 10 atm (higher pressure was not allowed because of the possibility of damage to the cell), into the free volume of the cell with the degassed water. (The degassing was accomplished by the routine described above.) Immediately after sealing, the cell was intensely shaken to facilitate effective penetration of He atoms into the liquid. After settling for a day (during this time, the liquid was saturated with He), the cell was again connected to the backing pump, but now the liquid sample was evacuated for 2 h. During this process, atoms of He escaped from liquid; this process was accompanied by vigorous boiling. After sealing the cell, we verified the pressure, p_{sat}, established inside the free volume and measured the value of W_{exp} (the experimental conditions for these measurements were the same as above); this value was slightly less than that before the "helium-washing" procedure. In the following stages of helium washing, the intensity of boiling while evacuating the cell decreased, and in a certain stage, the boiling terminated; that is, the atoms of He left the liquid via diffusion kinetics. The results of measurements of $W_{exp}(N_{hel})$ are plotted in Figure 7, where N_{hel} denotes the number of successive helium washings. The data show that the breakdown probability tends to zero at $N_{hel} = 5$ to 6, and boiling is terminated at the same numbers. As follows from the experimental graphs given above, the data on W_{exp} are characterized by a significant experimental scatter. At the same time, for the case of helium-washing-processed samples, the experimental scatter diminishes as the number of N_{hel} grows, tending to zero at $N_{hel} = 7$ to 8. The electric resistance of helium-washed samples and nonprocessed samples is the same (within the accuracy of measurements).

Therefore, this experiment showed that the atoms of He can remove the long-lived solvates of air molecules from the traps within the solvent matrix, and the low-threshold optical breakdown in water is initiated by such long-lived solvates. We can imagine that the atoms of He destroy these hypothesized long-lived solvates. The reason for such impact of helium atoms might be the following. First, as shown in ref 61, hydrophobic

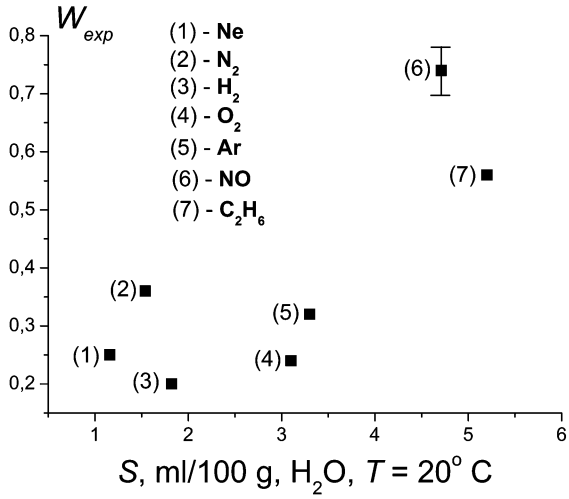

Figure 8. Value of probability, W_{exp}, measured after saturation of the water sample by gases of various solubility in water, followed by the "helium-washing" routine.

hydration is impossible for He in water. Additionally, the He atom is the smallest among all other monatomic gases; its radius in water is equal to 1.08 Å, whereas, for example, we have 1.21 Å for Ne, and 1.64 Å for Ar (see, e.g., ref 62). It is seen that the radius of He is less than the distance $d_{O-H\cdots O} = 2.82$ Å between hydrogen-bonded atoms of oxygen in liquid water at room temperature;[63] that is, the He atoms are easily able to occupy interstitials between molecules of water. We also remark that unlike all other gases, only dissolution of He in water is accompanied by the growth of enthalpy. (See ref 64.)

We tested the characteristics of helium-washed aqueous samples via dissolution in some other gases having different solubility. These experiments were carried out as follows: the chosen gas at pressure of $p = 1$ atm and temperature $T = 20$ °C was pumped into the free volume of the cell containing a water sample that had been subjected to a preliminary "wash" with helium.[73] Then, the sample was saturated with this gas for 24 h. Then, the magnitude of W_{exp} was measured for this sample. These results are summarized on the diagram in Figure 8; the abscissa corresponds to the solubility of the given gas in water scaled in mL per 100 g of the solvent at the room temperature; these data were taken from ref 65 and confirmed (within the experimental accuracy) by measuring the residual pressure in the free volume of the cell after saturating the liquid by the given gas. We can see that there exist noticeable differences in the magnitudes of W_{exp} for the different gases exhibited on this graph. In fact, the dependence of W_{exp} versus the solubility of gas looks nonmonotonic. However, with increasing the solubility in Figure 8, a general trend of rising W_{exp} can be beheld, albeit with strong gas-specific perturbations around the general trend. These perturbations may be coupled to gas-specific polarizability of molecules. For example, higher polarizabilities of N_2 compared with H_2 (1.74 vs 0.79 Å^3) or of Ar compared with O_2 (1.63 vs 1.57 Å^3) correspond to higher values of W_{exp} in Figure 8.

We assume that the molecules of gas, adsorbed into a liquid through its interface, have two kinds of solubility. The first type is the structural solubility: such molecules are ideally built in a matrix of the solvent and do not participate any more in the process of diffusion; it is possible to hypothesize that such molecules form a sort of a "sub-lattice" of the solvent matrix. We note also that the state of "structurally dissolved" gas molecule should be considered as a metastable one. This state is characterized by an instant mutual configuration of a nonpolar gas molecule and its molecular environment; such a configuration, obviously, has the limited lifetime.

The second kind of solubility can be termed diffusion solubility, wherein the gas molecules are capable of making diffusion movements inside the solvent. The opportunity of diffusion motion for such molecules is caused by the fact that these molecules serve as local defects of structure of the solvent. Such defects can be generated by hydrophobic molecules of the dissolved gas; that is, these gas molecules should disturb the proximal environment of molecules of the solvent. Hydrophobic hydration depends critically on the radius of the hydrophobic molecule and its orientation in the dynamic network of hydrogen bonds of the nearest neighboring molecules of water (see, e.g, ref 66). (At least, in the absence of any theory of water that includes many body aspects of "hydrogen bonding", this is the classical picture.) Therefore, this effect is critical to the type of dissolved gas. Because the occurrence of a local defect implies an increase in the free energy of the system, the presence of a gas molecule that disturbs local structure of the solvent is energetically unfavorable; such molecules should effectively be pushed out of the solvent matrix. The latter provides the necessary activation energy for launching the diffusion process for such molecules.

The molecule of gas, which correspond to the second type of solubility, can form a long-living Coulombic complex with a dissolved ion because of the dipole−monopole attractive interaction and because of specific ion dispersion interactions with water. Therefore, we obtain a charged long-living defect within the solvent matrix, which can play a role as a center for nucleation of a bubston. Therefore, we can assume that the volumetric rate of bubston generation should be proportional to the product $n_i \cdot n_g$, where n_i is density of the dissolved ions and n_g is the density of the gas molecules related to the second type of solubility. The argument is qualitative only. Such phenomena also involve not only electrostatic but also many body quantum mechanical intermolecular (dispersion) forces. (See ref 20.) (Recognizing this, it is clear that such induced and permanent dipole-induced dipole interactions should be ion-specific. This circumstance provides a key to the explanation of our previous results on ion-specific effects related to bubston clusters in aqueous solutions of various salts.[49]) It is noteworthy that the atom of He has the lowest atomic polarizability among all other gases due to its peculiar quantum mechanical properties (see, e.g., ref 67). Indeed, the atomic polarizability for He is 0.2×10^{-24} cm^{-3}, for Ne is 0.4×10^{-24} cm^{-3}, and for Ar is 1.6×10^{-24} cm^{-3}. Therefore, the potential well of dipole−monopole attraction for the atom of He is very shallow, and the lifetime of the Coulombic complex consisting of this atom and an ion is too small to form a long-lived bubston nucleus at room temperature. This is why the helium-washing routine results in essential decrease in the content of bubstons in a liquid sample.

In what follows, we describe some experiments that probe the properties of water samples processed by the helium-wash routine.

2.5. Experiment on Superheating. We carried out an experiment on measuring the boiling temperature of water, repeatedly processed by helium-washing routine. The number of such procedures was dictated by the condition of complete suppressing of the optical breakdown (Figure 7) and as a rule was within 8−12.

The open cell containing a sample of the helium-washed water (we used the same cell as that used previously) was placed inside a chamber, which was previously evacuated. The pressure inside

the chamber was preset with helium and fixed at a level of $p = 1$ atm; the open cell was connected to a heater. To avoid possible contamination of the sample, we did not measure the temperature directly inside the liquid; a thermoresistor was placed in quartz capillary attached to the face of the cell from the outside, so we actually measured the temperature of the heater. To avoid an increase in pressure due to evaporation of water, a Peltier cooler was mounted above the opening of the cell, and the vapor molecules were sublimated on the cooler interface. We controlled the pressure inside the chamber during the entire experiment; therefore, deviations of the pressure from 1 atm can be ignored. The cell was supplied with a piezoelectric sensor (described in ref 59) connected to Tektronix TDS-540 digital store oscilloscope. Within the temperature range $\Delta T = 160-170$ °C, the oscilloscope indicated bursts of acoustic pulses; the intensity of the acoustic signals practically did not change as the temperature increased. At the same time, a surface of the liquid sample began to demonstrate sharp jumps, but liquid remained absolutely transparent; that is, we did not see bubble boiling. The further increase in temperature of the heater did not result in a change of this mode. Although apparent indications of boiling were not observed (the water interface remained flat and no large bubbles formed), we associate these acoustic pulses and the surface jumps with the initiation of a special regime of boiling in the liquid, which was free of heterogeneous boiling centers. The temperatures for which the jumps of the liquid interface became observable are still far from the spinodal temperature. Indeed, for water at atmospheric pressure, the spinodal temperature, T_s, is equal to ~330 °C (see, e.g., the study[68] and references therein); such temperature was not achieved in our experiments. Note that the quoted value of T_s is the result of theoretic simulations; at the present, the maximal experimentally achieved superheating of water at atmospheric pressure is on the level of 303−310 °C, where the heating is produced by pulses of electric current in a thin wire, and the liquid is considered to be superheated if the explosive boiling does not occur during 1 to 2 s after termination of a current pulse. Our experiments on superheating are ongoing, and the results are preliminary. However, at this point, we can state the following. We do observe that the water samples, repeatedly processed by helium washing, are able to withstand higher temperatures of superheating, compared with the nonprocessed samples.

2.6. Experiment on Induction of Optical Breakdown. We carried out measurements of optical breakdown threshold, the structure of the breakdown flash, and the spectrum of that flash for samples of water processed by the helium-wash routine and for the nonprocessed samples. First of all, for the induction of optical breakdown in the water sample exposed to successive helium-wash processing, the laser pulse intensity is expected to increase by one to two orders of magnitude. As a matter of fact, in accordance with the results of study,[57] the optical breakdown can be induced in a liquid either because of the presence of heterogeneous breakdown centers or because of the multiphoton ionization of molecules of the liquid. Because the breakdown centers (solid microinclusions together with the clusters of bubstons) have been removed beforehand, the breakdown can be initiated only by the second mechanism. Bearing in mind that the intra-atomic electric field strength is $E \approx 10^8$ V/cm, we should substitute this magnitude into the formula for the intensity of laser radiation $I = E^2 n \varepsilon_0 c$, where n is the linear refractive index of water, $n = 1.33$, ε_0 is the permittivity of free space, and c is the vacuum speed of light; in that case, the nonlinear (multiphoton) ionization can occur. After substituting, we arrive at $I \approx 10^{12}$ to 10^{13} W/cm^2. However, we could not achieve such an intensity by using the Q-switching pulse-repetition laser of pulsewidth $\tau = 11$ ns, as described above. This was because for this situation we should increase the energy of pulse correspondingly (provided that the focusing conditions remain fixed). This was problematic. This is why for the helium-washed experiment we used a laser of wavelength $\lambda = 1.064$ μm operated in the mode-locking single-pulse regime; the pulsewidth, τ, was 21 ps. The maximum output energy of a single pulse selected from a train of pulses and subjected to two-cascade amplification was 10 mJ, the spectral width was 1 cm^{-1}, and the output beam diameter was 1 mm. The experimental setup is schematically shown in Figure 9. The laser beam was directed to a cell with the test water by the lens L1. The radiation scattered at 90° was detected by a mini-spectrometer supplied with an optical-fiber input.

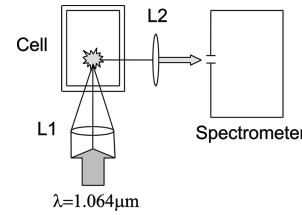

Figure 9. Schematic setup for investigating an optical breakdown in a water-filled cell.

In this study, we detected the optical breakdown threshold via the scattered incident laser radiation from the caustic at an angle of 90°. Figure 10a,b shows the dependence of the energy, I_s, of the scattering signal of incident radiation as a function on the laser energy; the incident radiation was focused by a lens L1 with focal length 70 mm into a cell with the water sample. Comparison of the plots shows that the breakdown threshold depends strongly on the dissolved gas content. For nonprocessed water, presumed to contain a large number of bubston clusters, the optical breakdown threshold with respect to the incident laser pulse energy was found to be $W_{th} = 0.07$ mJ. At the same time, for helium-washed water samples, the optical breakdown was $W_{th} = 0.9$ mJ. In both cases, the breakdown flash was observed visually as the pulse energy exceeded the threshold. The big experimental scatter of the dependence in Figure 10b indicates that breakdown in nonprocessed water is initiated by the breakdown centers. We see that under the same conditions the breakdown threshold energy for nonprocessed water is ten times lower than that for processed water. We remark that the self-focusing effect should reveal itself at high optical intensities (see, e.g., ref 69), resulting in an additional increase in intensity in the case of shooting processed water. Because we do not know the precise value of the beam cross-section in the focal area in that case, we cannot estimate the intensity and give the threshold values in the energy units.

Figure 11 shows a photo of the pattern of the breakdown flash in a processed water sample; the pressure inside the cell was 1 atm, which was achieved by letting 1 atm of helium into the free volume of the cell. It is interesting to compare this pattern with that of nonprocessed sample. (See Figure 2.) It is worth noting that the focusing conditions were the same in both cases. The light intensity for the pattern in Figure 2 was $I \approx 10^9$ W/cm^2, whereas, in the case of Figure 11, the intensity was equal to $I \approx 10^{13}$ W/cm^2. Both photos were taken with the help of the same micro-objective. The pattern of breakdown flash for the processed sample differs from that for the nonprocessed sample. First, we can see the tracks of the light cone beams in

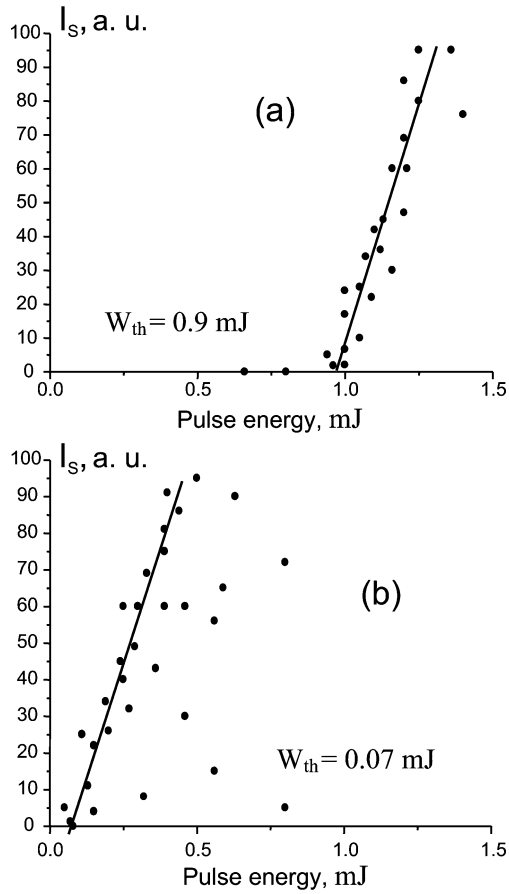

Figure 10. Dependence of the energy, I_s, of incident laser radiation scattered at an angle of 90° to the optical axis (in relative units) on the pulse energy for (a) helium-washing-processed and (b) nonprocessed water. The dots correspond to the experimental data.

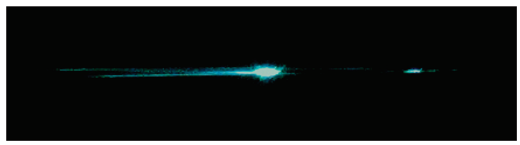

Figure 11. Photo of the breakdown flash in the processed sample of water.

the caustic as a result of the frequency up-conversion effect specific for very intense optical fields (see ref 69), whereas the radiation at the wavelength of $\lambda = 1.064$ μm is naturally invisible. Second, the breakdown has the form of a single, very bright flash of plasma, which almost completely shields the radiation. The upper and lower beams of the light cone had insufficient time for shielding. They managed to pass behind this plasma and gave rise to another, weaker plasma flash. As was demonstrated in other specific experiments, no radiation goes through the plasma region in this case; that is, we deal with complete shielding.

The breakdown flash spectra were also analyzed according to the scheme shown in Figure 9. Radiation was focused into the cell by the lens L1 with the focal length F1 = 17 mm. The light of the flash was projected by the lens L2 onto the entrance slit of the mini-spectrometer, which allowed us to record spectra in the spectral range from 180 to 1100 nm. The spectra of flashes are shown in Figure 12. A characteristic feature is the presence of pronounced lines in the spectra of processed water. These spectra are basically characterized by single narrow line with a width at half-maximum of about 50 nm. (Spectra with two or more peaks were extremely rare.) As far as we know, this is

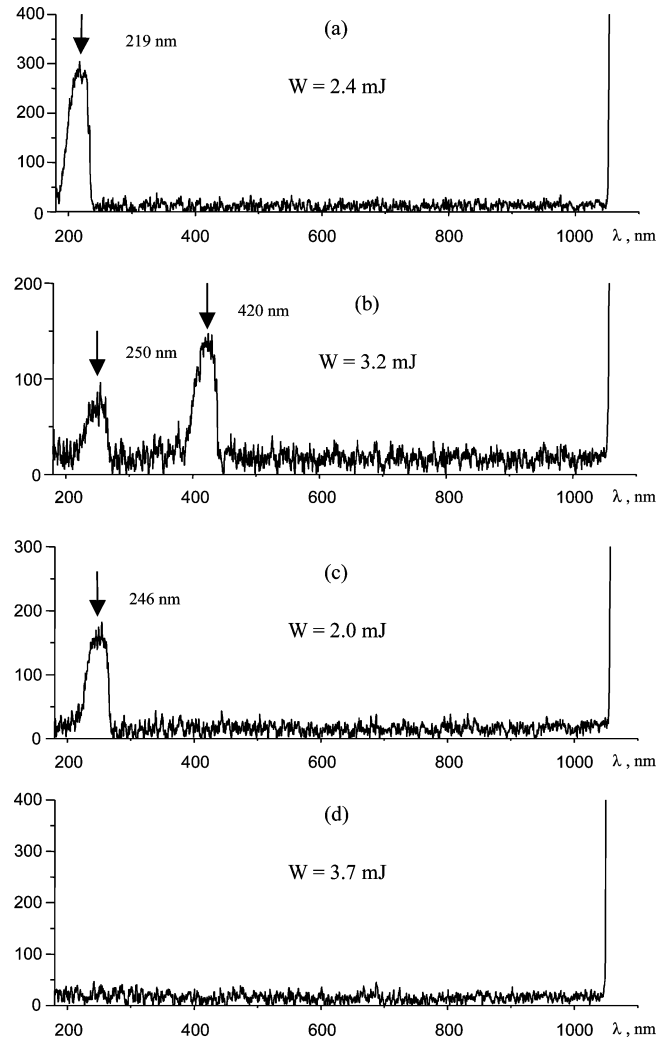

Figure 12. Spectra of individual flashes for the (a−c) helium-washing-processed and (d) nonprocessed water; W is the laser pulse energy in millijoules.

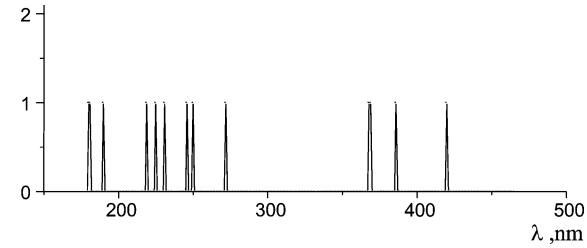

Figure 13. Diagram of the positions of lines in the flash spectrum for multiphoton breakdown of the helium-washing-processed water.

the first observation of isolated spectral lines in the flash of optical breakdown, induced by a laser pulse at the wavelength of $\lambda = 1.064$ μm for the picosecond time scale. The only mechanism capable of inducing optical breakdown with such peculiarities of the flash spectrum is related to the multiphoton ionization of water molecules. (See ref 57.) Assuming a value of 6.5 eV for the bulk ionization potential of water,[70] we estimated that five to six photons are necessary for inducing multiphoton breakdown in water at $\lambda = 1.064$ μm.

As to the breakdown of nonprocessed water, supposing it contains clusters of bubstons, such intense spectral components were absent. At the same time, the flash of plasma radiation could be visually observed in that case, as well. (See Figure 2.) As further analysis showed, the flash spectrum in that case was

TABLE 1: Experimental Data on Breakdown Spectra in the Helium-Washing-Processed Water

peak position (experiment) Λ_{max}, nm (±1 nm)	spectral absorption bands of molecular and ionic complexes and indication of electronic terms, λ, nm
180, 190	175−535, O_2, Schuman−Runge band, $B^3\Sigma_u^- - X^3\Sigma_g^-$; 194−653, O_2^+
219, 225, 231, 246, 250, 272	175−535, O_2, Schuman−Runge band, $B^3\Sigma_u^- - X^3\Sigma_g^-$; 194−653, O_2^+, $A^2\Pi_u - X^2\Pi_g$; 260−410, OH, $A^2\Sigma^- - X^2\Pi$
368, 369, 386	260−410, OH, $A^2\Sigma^- - X^2\Pi$; 254−479, O_2, Herzberg II band, $C^1\Sigma_u - X^3\Sigma_g^-$
420	421−566, OH, $B^2\Sigma^+ - A^2\Sigma$; 370−438, O_2, Herzberg III band, $C^3\Delta_u - a^1\Delta_g$

almost continuous. The continuous character of the spectrum can be due to the electron bremsstrahlung in the separate bubstons of cluster, in agreement with the results of the theory.[56] In fact, for observing the bremsstrahlung spectral line, the large time of accumulation of the bremsstrahlung signal is required; that is, large number of laser pulses must be shot to detect this line. We should emphasize that in the experiment described here the spectral patterns were obtained for a single pulse. This is why the bremsstrahlung line is absent in Figure 12d; the bremsstrahlung spectral intensity in a single pulse was insufficient for detection by our mini-spectrometer.

Figure 13 shows a diagram with the positions of maxima observed in the processed water breakdown spectrum. These data were obtained from observations of 20 breakdown flashes and compiled in Table 1. Additionally, Table 1 contains the known absorption bands for the molecular and ionic complexes,[71] with indication of the corresponding transitions between electronic terms. Naturally, all peaks in the breakdown spectra of processed water can be related to the electronic transitions in the particles indicated in the right column of Table 1.

Obviously the correspondence between the experimental results and tabular data is not as good as one would desire. The dominance of particular spectral bands in the left column of Table 1 depends on many factors. They include, for example, the distribution of the populations of vibration sublevels of the excited electronic state (effective temperature), and the probabilities of transitions between individual vibrational sublevels of the particular electronic state. In this case, an uncontrollable factor for optical breakdown in water via multiphoton ionization is the temperature of the plasma. This is obviously related to the fact that the regime of heat exchange between the plasma and surrounding liquid cannot be steady for times of ~21 ps. Therefore, the distribution of population of vibrational sublevels of the excited electronic state is not reproduced from pulse to pulse; besides, the energy fluctuations in pulses should also contribute. These factors explain the poor reproducibility in the spectral measurements.

3. Summary

We have demonstrated that in water free of external solid impurities, the molecules of dissolved gas exert critical influence on both optical breakdown and boiling. The effects are gas-molecule- and gas-content-specific. Of course, the fact that dissolved gas affects the boiling point of water is long known. What is of interest is how that reflects structure and aggregation of gas molecules within water.

The gas solute molecules can be almost completely removed via the routine of helium wash. On the basis of the experimental results, we can say that the water samples, processed by the helium-washing routine, essentially differ from the nonprocessed samples with respect to the optical breakdown threshold, the geometric characteristics of the breakdown flash, the effect of shielding, the spectral characteristics of the breakdown flash, and the boiling temperature. The explanation for such dissimilarities essentially lies in the removal of the centers for optical breakdown and boiling from the processed samples. As a result, for the processed samples, the breakdown mechanism implies the multiphoton ionization of the liquid molecules, whereas for the nonprocessed samples, this mechanism is the low-threshold electron avalanche inside separate bubstons of a cluster.

Regardless of this, our favored interpretation of the helium-washing technique should be of value in obtaining effectively degassed water free of microstructure and clathrates for many applications in colloid science that involve interactions.

Acknowledgment. This work was supported by the Russian Foundation for Basic Researches, grant no. 10-02-00377-à. We thank Mr. A. V. Shkirin for fruitful discussions and technical support in preparing the manuscript.

References and Notes

(1) Collins, K. D.; Washabaugh, M. W. *Q. Rev. Biophys.* **1985**, *18*, 323–422.
(2) Kunz, W.; Lo Nostro, P.; Ninham, B. W. *Curr. Opin. Colloid Interface Sci.* **2004**, *9*, 1–18.
(3) Bostrom, M.; Williams, D. R.; Ninham, B. W. *Langmuir* **2002**, *18*, 8609–8615.
(4) Lo Nostro, P.; Fratoni, L.; Ninham, B. W.; Baglioni, P. *Biomacromolecules* **2002**, *3*, 1217–24.
(5) Zhang, Y.; Cremer, P. S. *Curr. Opin. Chem. Biol.* **2006**, *10*, 658–663.
(6) Du, Q.; Freysz, E.; Shen, Y. R. *Science* **1994**, *264*, 826–829.
(7) Scatena, L. F.; Brown, M. G.; Richmond, G. L. *Science* **2001**, *292*, 908–912.
(8) Vaitheeswaran, S.; Rasaiah, J. C.; Hummer, G. *J. Chem. Phys.* **2004**, *121*, 7955–7965.
(9) Vácha, R.; Slavíek, P.; Mucha, M.; Finlayson-Pitts, B. J.; Jungwirth, P. *J. Phys. Chem. A* **2004**, *108*, 11573–11579.
(10) Ohshima, H.; Healy, T. W.; White, L. R. *J. Colloid Interface Sci.* **1982**, *90*, 17–26.
(11) Gan, W.; Wu, D.; Zhang, Z.; Guo, Y.; Wan, H. *Chinese J. Chem. Phys.* **2006**, *19*, 20–24.
(12) Smits, M.; Ghosh, A.; Sterrer, M.; Müller, M.; Bonn, M. *Phys. Rev. Lett.* **2007**, *98*, 098302.
(13) Bosma, W. B.; Fried, L. E.; Mukamel, S. *J. Chem. Phys.* **1993**, *98*, 4413–4421.
(14) Jedlovszky, P.; Mezei, M.; Vallauri, R. *Chem. Phys. Lett.* **2000**, *318*, 155–160.
(15) Thomas, A. S.; Elcock, A. H. *J. Am. Chem. Soc.* **2007**, *129*, 14887–14898.
(16) Van der Spoel, D.; Van Maaren, P. J.; Berendsen, H. J. C. *J. Chem. Phys.* **1998**, *108*, 10220–10230.
(17) Bruge, F.; Bernasconi, M.; Parrinello, M. *J. Am. Chem. Soc.* **1999**, *121*, 10883–10888.
(18) Xenides, D.; Randolf, B. R.; Rode, B. M. *J. Mol. Liq.* **2006**, *123*, 61–67.
(19) Landau, L. D.; Lifshitz, E. M. *Electrodynamics of Continuous Media*; Pergamon: Oxford, U.K., 1960.
(20) Ninham, B. W.; Lo Nostro, P. *Intermolecular Forces and Self Assembly in Colloid, Nano Sciences and Biology*; Cambridge University Press, New York, 2010.
(21) Massoudi, R.; King, A. D. *J. Phys. Chem.* **1974**, *78*, 2262–2266.

(22) Petersen, P. B.; Johnson, J. C.; Knutsen, K. P.; Saykally, R. J. *Chem. Phys. Lett.* **2004**, *397*, 46–50.
(23) Petersen, P. B.; Saykally, R. J. *J. Am. Chem. Soc.* **2005**, *127*, 15446–15452.
(24) Petersen, P. B.; Saykally, R. J. *Annu. Rev. Phys. Chem.* **2006**, *57*, 333–364.
(25) Garrett, B. C. *Science* **2004**, *303*, 1146–1147.
(26) Knipping, E. M.; Lakin, M. J.; Foster, K. L.; Jungwirth, P.; Tobias, D. J.; Gerber, R. B.; Dabdub, D.; Finlayson-Pitts, B. J. *Science* **2000**, *288*, 301–306.
(27) Dougherty, R. C. *J. Phys. Chem. B* **2001**, *105*, 4514–4519.
(28) Stevens, H.; Considine, R. F.; Drummond, C. J.; Hayes, R. A.; Attard, P. *Langmuir* **2005**, *21*, 6399–6405.
(29) Meyer, E. E.; Lin, Q.; Israelachvili, J. N. *Langmuir* **2005**, *21*, 256–259.
(30) Pashley, R. M.; Rzechowicz, M.; Pashley, L. R.; Francis, M. J. *J. Phys. Chem. B* **2005**, *109*, 1231–1238.
(31) Meagher, L.; Craig, V. S. J. *Langmuir* **1994**, *10*, 2736–2742.
(32) Considine, R. F.; Hayes, R. A.; Horn, R. G. *Langmuir* **1999**, *15*, 1657–1659.
(33) Pashley, R. M. *J. Phys. Chem. B* **2003**, *107*, 1714–1720.
(34) Wennerstrom, H. *J. Phys. Chem. B* **2003**, *107*, 13772–13773.
(35) Karaman, M. E.; Ninham, B. W.; Pashley, R. M. *J. Phys. Chem.* **1996**, *100*, 15503–15507.
(36) Craig, V. S. J.; Ninham, B. W.; Pashley, R. M. *Langmuir* **1999**, *15*, 1562–1569.
(37) Craig, V. S. J.; Ninham, B. W.; Pashley, R. M. *J. Phys. Chem.* **1993**, *97*, 10192–10197.
(38) Ivanov, E. V.; Lebedeva, E. J.; Abrosimov, V. K.; Ivanova, N. G. *J. Struct. Chem.* **2005**, *46*, 253–263.
(39) Scharlin, P.; Battino, R.; Silla, E.; Tunon, I.; Pascual-Ahuirc, J. L. *Pure Appl. Chem.* **1998**, *70*, 1895–1904.
(40) Wilhelm, E.; Battino, R.; Wilcock, R. J. *Chem. Rev.* **1977**, *77*, 219–262.
(41) Duffy, J. R.; Smith, N. O.; Nagy, B. *Geochim. Cosmochim. Acta* **1961**, *24*, 23–31.
(42) Smith, N. O.; Kelemen, S.; Nagy, B. *Geochim. Cosmochim. Acta* **1962**, *26*, 921–926.
(43) Hermann, C.; Dewes, I.; Schumpe, A. *Chem. Eng. Sci.* **1995**, *50*, 1673–1675.
(44) Rischbieter, E.; Stein, H.; Schumpe, A. *J. Chem. Eng. Data* **2000**, *45*, 338–340.
(45) Stoessel, R. A.; Byrne, P. A. *Geochim. Cosmochim. Acta* **1982**, *46*, 1327–1332.
(46) Brennen, C. E. *Cavitation and Bubble Dynamics*; Oxford University Press: New York, 1995.
(47) Anderson, T. L. *Fracture Mechanics: Fundamentals and Applications*; CRC Press: Boca Raton, FL, 1995.
(48) Lauterborn, W. *Cavitation and Inhomogeneities in Underwater Acoustics*; Springer Verlag: New York, 1980; Chapter 1.
(49) Bunkin, N. F.; Kiseleva, O. A.; Lobeyev, A. V.; Movchan, T. G.; Ninham, B. W.; Vinogradova, O. I. *Langmuir* **1997**, *13*, 3024–3028.
(50) Bunkin, N. F.; Lobeyev, A. V.; Lyakhov, G. A.; Ninham, B. W. *Phys. Rev. E* **1999**, *60*, 1681–1690.
(51) Bunkin, N. F.; Kochergin, A. V.; Lobeyev, A. V.; Ninham, B. W.; Vinogradova, O. I. *Colloids Surf., A* **1996**, *10*, 207–212.
(52) Vinogradova, O. I.; Bunkin, N. F.; Churaev, N. V.; Kiseleva, O. A.; Lobeyev, A. V.; Ninham, B. W. *J. Colloid Interface Sci.* **1995**, *173*, 443–447.
(53) Bunkin, N. F.; Bunkin, F. V. *Sov. Phys. - JETP* **1992**, *74*, 271.
(54) Bunkin, N. F.; Bunkin, F. V. *J. Exp. Theor. Phys.* **2003**, *96*, 730.
(55) Bunkin, N. F.; Suyazov, N. V.; Shkirin, A. V.; Ignatiev, P. S.; Indukaev, K. V. *J. Chem. Phys.* **2009**, *130*, 134308.
(56) Bunkin, N. F.; Bunkin, F. V. *Laser Phys.* **1993**, *3*, 63.
(57) Kennedy, P. K.; Hammer, X.; Rockwell, B. A. *Prog. Quantum Electron.* **1997**, *21*, 155.
(58) Vogel, A.; Lauterborn, W. *Appl. Opt.* **1988**, *27*, 1869.
(59) Veselovskii, I. A. *Akust. Zh.* **1987**, *33*, 834.
(60) Cole, R. H. *Underwater Explosions*; Princeton University: Princeton, NJ, 1948.
(61) Graziano, G. *J. Chem. Soc., Faraday Trans.* **1998**, *94*, 3345–3352.
(62) Zhang, Y.; Xu, Z. *Am. Mineral.* **1995**, *80*, 670–675.
(63) Hydrogen Bonding in Water. http://www1.lsbu.ac.uk/water/hbond.html.
(64) Graziano, G. *J. Phys. Chem. B* **2001**, *105*, 2079–2081.
(65) *Handbook of Chemistry and Physics*, 86th ed.; CRC Press: Boca Raton, FL, 2005. http://encyclopedia.airliquide.com/.
(66) Southall, N. T.; Dill, K. A. *J. Phys. Chem. B* **2000**, *104*, 1326.
(67) Ashcroft, N. W.; Mermin, N. D. *Solid State Physics*; Saunders College Publishing: Fort Worth, TX, 1976; p 544, Table 27.1.
(68) Skripov, V. P. *Metastable Liquids*; Wiley: New York, 1972.
(69) Shen, Y. R. *The Principles of Nonlinear Optics*; John Wiley and Sons: New York, 1984.
(70) Boyle, J. W.; Chormley, J. A.; Hochanadel, C. J.; Riley, J. F. *J. Phys. Chem.* **1969**, *73*, 2886.
(71) Kuznetsova, L. A.; Kuz'menko, N. E.; Kuzyakov, Yu. Ya.; Plastinin, Yu. A. *Probabilities of Optical Transitions in Diatomic Molecules*; Nauka: Moscow, 1980 [in Russian].
(72) Note that we invoke here the Poisson distribution as we deal with alternative: the optical breakdown either occurs or does not. Because the number of random samplings (in our case, it is the number of laser shots in a series of a particular measurement of W_{exp}) is very high, we can use the Poisson distribution because it is an asymptotic to the binomial distribution, which is relevant for random processes implying the existence of alternative in outcomes.
(73) For these experiments, we employed ten cycles of helium washings. The criterion of sufficiency for such a number of cycles was the absence of optical breakdown prior to saturating with a test gas.

JP101657F